ACS APPLIED MATERIALS & INTERFACES

Research Article

www.acsami.org

Hydroxyl Functionalized Polytriazole-*co*-polyoxadiazole as Substrates for Forward Osmosis Membranes

Phuoc H. H. Duong,[†] Stefan Chisca,[†] Pei-Ying Hong,[†] Hong Cheng,[†,‡] Suzana P. Nunes,*[,†] and Tai-Shung Chung*[,§]

[†]Water Desalination & Reuse Center (WDRC), King Abdullah University of Science and Technology (KAUST), Thuwal 23955-6900, Saudi Arabia

[‡]Chongqing Institute of Green and Intelligent Technology, Chinese Academy of Sciences, Chongqing 401122, China

[§]Department of Chemical and Biomolecular Engineering, National University of Singapore, 4 Engineering Drive 4, Singapore 117585, Singapore

ABSTRACT: Hydroxyl functionalized polytriazole-*co*-polyoxadiazole (PTA–POD) copolymers have been synthesized and cast as promising highly thermally stable, chemically resistant, and antiorganic/biological fouling porous substrates for the fabrication of thin-film composite (TFC) forward osmosis (FO) membranes. The roles of PTA/POD ratios in the membrane substrates, TFC layers, and FO membrane performance have been investigated. This study demonstrates that the substrate fabricated from the copolymer containing 40 mol % PTA is optimal for the TFC membranes. Compared to the POD–TFC membrane, the 40 mol % PTA–TFC membrane exhibits a remarkable decrease in structural parameter (S) of more than 3.3 times. In addition, the 40 mol % PTA–TFC membrane is characterized by high water fluxes of 24.9 LMH and 47.2 LMH using 1 M NaCl as the draw solution and DI water as the feed under FO and pressure retarded osmosis (PRO) modes, respectively. Compared to a polysulfone (PSU) supported TFC-FO membrane under similar fabrication conditions, the 40% mol PTA–TFC membrane shows better FO performance and enhanced antifouling properties on the support (lower protein binding propensity and improved bacterial inhibition). Moreover, the performance of the 40 mol % PTA supported TFC-FO membrane can be improved to 37.5 LMH (FO mode)/78.4 LMH (PRO mode) and potentially higher by optimizing the support morphology, the TFC formation, and the post-treatment process. Hence, the use of newly developed hydroxyl functionalized polytriazole-*co*-polyoxadiazole copolymers may open up a new class of material for FO processes.

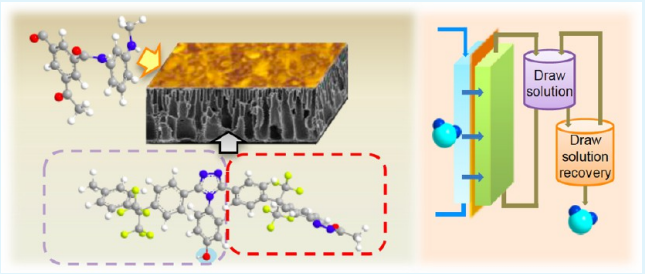

KEYWORDS: *polyoxadiazole, polytriazole, forward osmosis, membrane, water*

INTRODUCTION

Global scarcity of freshwater and environmental impacts of wastewater are becoming of great concern around the world. Separations of freshwater from other contaminants by membrane-based processes are proven technologies. Membrane-based processes for water treatment and seawater desalination can be classified into (i) pressure-driven membrane processes including microfiltration (MF), ultrafiltration (UF), nanofiltration (NF), and reverse osmosis (RO);[1−5] and (ii) osmotically driven membrane processes such as forward osmosis (FO).[6−8] While RO has dominated for several decades as the state-of-the-art technology to remove trace contaminants in desalination and wastewater treatment, FO is an emerging technology in the same fields based on osmotically driven membrane processes.[6,9−16] Like RO, semipermeable membranes are used in FO processes to separate water from other contaminants. Comparing FO to RO for water treatment, FO is a naturally driven process that requires no or very low external hydraulic pressure. Hence, FO exhibits many potential advantages such as low fouling propensity,[17] easy cleaning,[17−19] low equipment costs,[6] and higher water recovery.[20]

Despite the aforementioned advantages, the lack of sufficient membranes is one of the critical challenges that hinder the development of FO technology. A huge research effort has been focused on developing a new generation of FO membranes with high performance and excellent stabilities. In general, a FO membrane contains an asymmetric structure with a thin active layer that plays as a contaminant rejection layer and a porous support layer that provides the mechanical support to the thin active layer. Various studies on the thin active layer have been focused to increase the FO performance and fouling resistance.[21−27] Besides, the design of the porous support has extensively been studied using a wide range of polymers (i.e., cellulose acetate, cellulose triacetate, poly(ether sulfone) (PES), polysulfone (PSU), polyacrylonitrile (PAN), polybenzimida-

Received: September 10, 2014
Accepted: February 4, 2015
Published: February 4, 2015

DOI: 10.1021/am508387d
ACS Appl. Mater. Interfaces 2015, 7, 3960−3973

(a) Polyoxadiazole (POD)

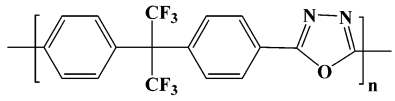

(b) Hydroxyl functionalized polytriazole-co-polyoxadiazole (PTA–POD)

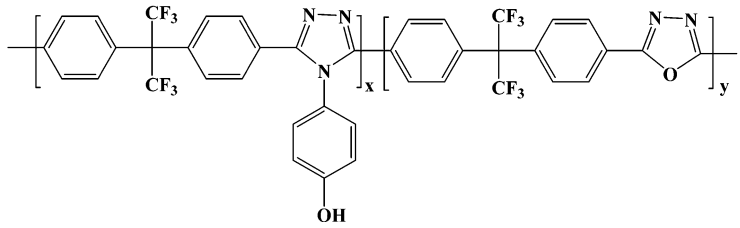

Figure 1. Molecular structures of (a) polyoxadiazole (POD) and (b) hydroxyl functionalized polytriazole-*co*-polyoxadiazole (PTA–POD).

zole (PBI), nylon-6,6; polyvinylidene fluoride (PVDF), polyamide-imide, and their deviations) to achieve highly porous FO membranes with minimal concentration polarization.[28−31] Despite increased efforts to investigate highly stable FO membranes, most of the fabricated membranes do not possess high thermal, chemical, and mechanical stabilities which may limit the fields of applications and the lifetime of membranes.

Among polymers for membrane fabrication, polyoxadiazoles (PODs) have gained attention as promising stable membrane materials[32−34] because of their excellent thermal, oxidative, and mechanical stability.[35] However, this class of materials exhibits high hydrophobicity which is an unfavorable property for the fabrication of FO membranes. Another type of polyazoles—polytriazoles (PTAs), which are more hydrophilic than PODs but contain all aromatic and heterocyclic in their structure, exhibits good thermal stability, chemical resistance, and tough mechanical properties. Therefore, various studies have been carried out to fabricate gas separation,[36] membrane distillation,[33] and proton conductive[37,38] membranes from PTAs. In addition to their promising stabilities, POD and PTA membranes may also play as good antifouling membranes in water treatment applications due to the antibiofouling properties of oxadiazoles,[39] and antifungal[40−42] and antifouling[43] properties of triazoles. Until now, the applications of PODs and PTAs on membrane fabrication via the phase-inversion technique are still limited due to their low solubility in common casting solvents (i.e., *N*-methyl-2-pyrrolidone, dimethylformamide, dimethylacetamide) that reduces the polymer processability. Furthermore, the lower hydrophilicity of PODs and PTAs can be another reason that these polymers have not been studied for fabricating FO membranes.

For the first time, in this paper, we introduce a new type of polyazoles, hydroxyl functionalized polytriazole-*co*-polyoxadiazole (PTA–POD), as a potential material for fabricating FO support membranes. Our strategy is to utilize the advanced properties of POD and PTA polymers with the aid of the hydroxyl modification to obtain hydrophilic PTA–POD copolymers with good solubility in common organic solvents while maintaining the high stabilities of POD and PTA. With enhanced hydrophilicity and solubility, the newly synthesized PTA–POD copolymers may become suitable materials for fabricating stable FO support membranes. The objectives of this study are to (i) investigate the effect of hydroxyl-functionalized PTA content in the PTA–POD copolymer on the morphology and transport properties of the flat-sheet substrates via the phase-inversion process; (ii) study the effect of hydroxyl-functionalized PTA content in TFC membrane substrates on FO performance; (iii) examine the promising properties of the hydroxyl-functionalized PTA substrate in antifouling and FO performance by comparison to a conventional PSU substrate under similar fabrication conditions; and (iv) demonstrate the possibility of fabricating a high performance TFC FO membrane from the hydroxyl-functionalized PTA substrate by turning substrate morphology, TFC formation, and post-treatment conditions.

MATERIALS AND METHODS

Materials. Polyoxadiazole (POD) and hydroxyl functionalized polytriazole-*co*-polyoxadiazole (PTA–POD) polymers (Figure 1) were self-synthesized by polycondensation reactions[44] and utilized as raw materials for the fabrication of membrane supports using *N*-methyl-2-pyrrolidone (NMP, Sigma-Aldrich) as the solvent. A commercial available polysulfone (PSU, UDEL P-3500) was received from Solvay Advanced Polymers. Trimesoyl chloride (TMC), m-phenylenediamine (MPD), ethyl acetate, and n-hexane were obtained from Sigma-Aldrich and used for the synthesis of the thin film composite active layer (TFC) by interfacial polymerization. Sodium chloride (NaCl) was obtained from Merck (Germany). Isopropanol (IPA); polyethylene glycol 400, 10 000, and 35 000 (PEG, Mw = 400 g mol^{-1}, Mw = 10,000 g mol^{-1} and Mw = 35,000 g mol^{-1}); and poly(ethylene oxide) 100 000, 300 000, and 600 000 (PEO, Mw = 100 000 g mol^{-1} and Mw = 300 000 g mol^{-1}) were purchased from Sigma-Aldrich. Fluorescein isocyanate conjugated bovine serum albumin (BSA-FITC) and 2X LIVE/DEAD BacLight bacterial viability stains were obtained from Invitrogen.

Membrane Preparation. Asymmetric porous supports were fabricated from different dope solutions containing POD, PTA–POD, or PSU polymers by the conventional phase inversion method. Homogeneous casting solutions with a polymer concentration of 18 wt % in NMP were prepared from PSU and four types of copolymers containing various PTA percentages under continuous stirring conditions at 60 °C for 1 day. The porous supports were cast on a glass plate using a 100 μm gap casting knife, followed by immediate immersion in a water coagulant bath at room temperature. After complete coagulation, the as-cast membranes were kept in a water bath overnight for solvent removal.

Subsequently, the thin film composite layer (TFC) was deposited onto the top of porous supports by interfacial polymerization (IP) to form FO membranes. First, the supports were immersed in a 2 wt % MPD monomer aqueous solution for 5 min. After that, they were

DOI: 10.1021/am508387d
ACS Appl. Mater. Interfaces 2015, 7, 3960−3973

taken out from the solution followed by the removal of excess water droplets from the surface by tissue papers. Then, the supports were placed in frames so that only the top surfaces were exposed to the reactant. A 0.1% (w/v) TMC solution in hexane without (IP-I) or with the presence of 3% (v/v) ethyl acetate (IP-II) was poured onto the top surface of the support for 1 min to form a thin polyamide film via the polymerization reaction between MPD and TMC monomers. The freshly prepared TFC membranes were dried in open air at room temperature for 1 min and then rinsed with DI water several times to remove the unreactants. The resultant membranes were stored in DI water for further characterizations. All TFC membranes mentioned in this study were fabricated using the IP-I method unless specified. Some of the TFC-FO membranes were subjected to a post-treatment method by prewetting the membranes in an IPA/water (50/50, v/v) for 2 min.

Determinations of Pure Water Permeance (PWP), Molecular Weight Cutoff (MWCO), Mean Effective Pore Size (μ_p), and Pore Size Distribution of the Membrane Supports. The membrane substrates were immobilized into a lab-scale dead-end filtration setup to measure the pure water permeance (L m^{-2} h^{-1}/bar) and solute rejection at 5 bar under room temperature with an effective membrane area of approximately 12.56 cm^2. For the pure water permeance, the experiments were carried out using DI water as a feed. Subsequently, the mean effective pore size (μ_p), pore size distribution, and molecular weight cutoff of the supports were determined by solute separation experiments using aqueous feed solutions containing 100 ppm of various molecular weights of neutral solutes (PEG or PEO). The solute rejection (R) was calculated from the concentrations of the solute in the feed and permeate that were analyzed by a total organic carbon (TOC) analyzer (TOC-VCSH, Shimadzu, Japan).

From the known molecular weight (M) of a neutral solute, its Stokes diameter (d_s) was calculated in the following equations.[45,46]

For PEG

$$d_s = 33.46 \times 10^{-12} \times M^{0.557} \quad (1)$$

and for PEO

$$d_s = 20.88 \times 10^{-12} \times M^{0.587} \quad (2)$$

From the solute rejection and diameter, the mean effective pore size (μ_p), pore size distribution, and MWCO were determined by ignoring interactions between solutes and membrane pores. The mean effective pore size (μ_p) was determined at solute rejection R = 50%, and the geometric standard deviation (σ_p) gives an idea of how broad the pore size distribution is. It is defined as the ratio of d_s at R = 84.13% over that at R = 50%, analogously to the statistical description of nonuniform particle systems.[47] The MWCO is the molecular weight, which is 90% rejected by the membrane (R = 90%). On the basis of μ_p and σ_p, the pore size distribution of the membrane was conducted using the following probability density function:

$$\frac{dR(d_p)}{dd_p} = \frac{1}{d_p \ln \sigma_p \sqrt{2\pi}} \exp\left[-\frac{(\ln d_p - \ln \mu_p)^2}{2(\ln \sigma_p)^2}\right] \quad (3)$$

Membrane Porosity (ε) and Contact Angle of the Substrates. To determine the porosity (ε) of the membrane substrates, the weights of the wet membranes without excess water on the surface (m_1) were first determined followed by overnight vacuum-drying. The dried membranes were then reweighed (m_2, g) to determine the amount of absorbed water into the membrane pores and the polymer weight. From the known densities of both water (ρ_w) and polymers (ρ_p), the porosity of the membrane substrates ε was then obtained as follows:

$$\varepsilon = \frac{(m_1 - m_2)/\rho_w}{(m_1 - m_2)/\rho_w + m_2/\rho_p} \quad (4)$$

Prior to contact angle measurements, all membrane substrates were freeze-dried to remove water. All contact angle (θ) measurements were conducted using a Krüss Easydrop (Krüss GmbH, Germany) by advancing a small water volume of 1 μL onto the top surface of membrane substrates in the static mode at 23 ± 1 °C.

Morphology, Topology, and Interfacial Chemistry Characterizations of the Membranes. The membrane morphologies were observed under a field-emission scanning electron microscope (FESEM). Before imaging, the membranes were freeze-dried, fractured in liquid nitrogen, and then coated with iridium particles by an Emitech K575X sputter coater (Quorum Technologies, U.K.) for 30 s at 20 mA before imaging analyses. Subsequently, the membrane surface and cross-section morphologies were obtained with either a Quanta 600 FEG or a Nova NanoSEM 630 (FEI). Imaging was carried out at an acceleration voltage of 4−5 kV with a working distance of 4−9 mm.

Fourier transform infrared spectroscopy (FTIR) with the attenuated total reflectance (ATR) mode was utilized to characterize membrane surface chemistry. A PerkinElmer Spectrum 100 (PerkinElmer) equipped with a universal ATR was used for the spectra scanning over the range 400−1800 cm^{-1}. Data were collected over 16 scans with a resolution of 4 cm^{-1}.

An atomic force microscope (AFM) was employed to examine the surface topology of TFC membranes. A membrane area of 5 μm × 5 μm was visualized by an Agilent 5400 SPM microscope (Agilent Technologies) under the tapping-mode in air with a silicon AFM cantilever (Nanosensors, Switzerland). Furthermore, the quantitative roughness was calculated using the Pico Image software in terms of mean roughness (R_a) and root mean squared roughness (R_q).

Mass Transport Characteristics of TFC Membranes. The membranes' water permeance (A, L m^{-2} h^{-1} bar^{-1}), salt rejection (R_s, %), and salt flux (B, L m^{-2} h^{-1}) were determined by using a lab-scale dead-end filtration setup. The tests were carried out at 5 bar under room temperature with an effective membrane area of approximately 12.56 cm^2.

R_s values were determined by carrying out the tests using a 2000 ppm of NaCl solution as the feed under a rapid stirring condition (700 rpm). R_s was calculated with the following equation:

$$R_s = \left(1 - \frac{C_{p\text{-}s}}{C_{f\text{-}s}}\right) \times 100\% \quad (5)$$

Here $C_{f\text{-}s}$ and $C_{p\text{-}s}$ are the NaCl concentrations of the feed and the permeate, respectively. They were determined by conductivity measurements using a ProfiLine Cond 3310 conductivity (WTW, Germany).

The B values of membranes were determined from the solution-diffusion theory:

$$\frac{100 - R_s}{R_s} = \frac{B}{A(\Delta P - \Delta\pi)} \quad (6)$$

Here, ΔP is the applied pressure and $\Delta\pi$ is the osmotic pressure different across the membrane.

Evaluation of Forward Osmosis Performance. The performance of membranes was evaluated on a lab-scale cross-flow FO setup. The temperatures of the feed and draw solutions were kept at 23 ± 1 °C. The system was operated with a draw solution and a feed solution flowing countercurrently on each side of the membrane. The membrane performance was tested under both PRO (the TFC layer faced against the draw solution) and FO (the TFC layer faced against the feed solution) modes at various draw solution concentrations.

Water flux (J_v, L m^{-2} h^{-1}, abbreviated as LMH) and reverse salt flux (J_s, g m^{-2} h^{-1}, abbreviated as gMH) of the TFC membranes were measured using the following equations:

$$J_v = \frac{\Delta V}{A_{eff}\Delta t} \quad (7)$$

and

$$J_s = \frac{\Delta(C_t V_t)}{A_{eff}\Delta t} \quad (8)$$

DOI: 10.1021/am508387d
ACS Appl. Mater. Interfaces 2015, 7, 3960−3973

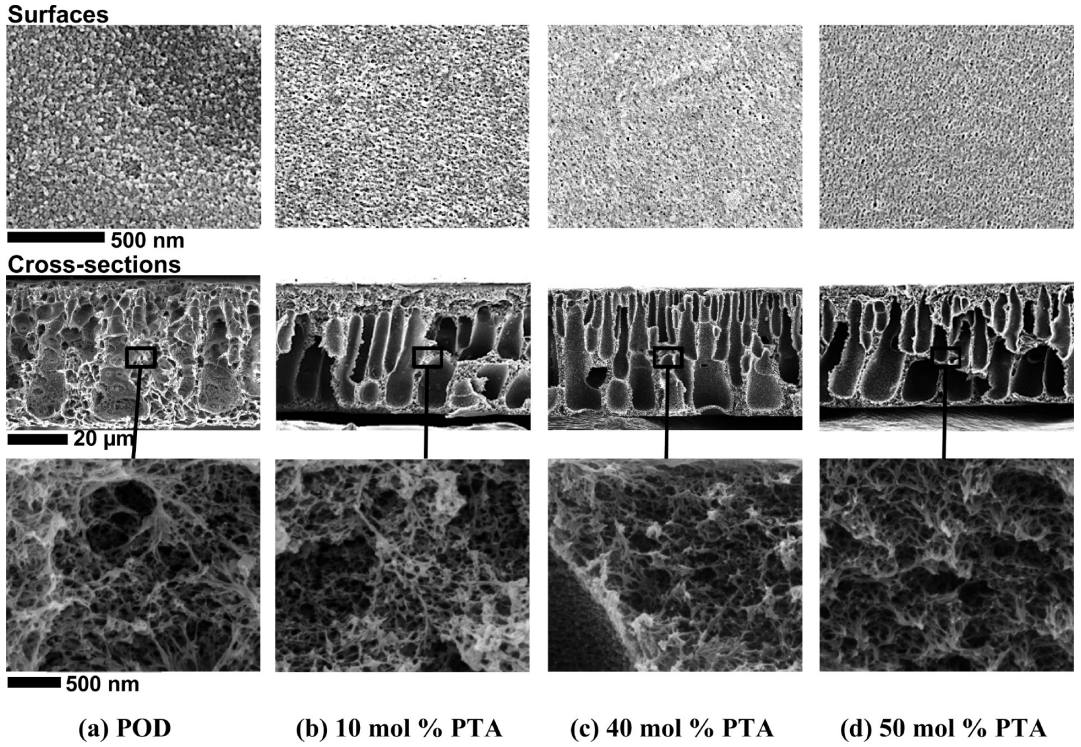

Figure 2. FESEM micrographs of surfaces and cross section images of (a) POD, (b) 10 mol % PTA, (c) 40 mol % PTA, and (d) 50 mol % PTA membrane substrates.

where ΔV (L) is the volume of water that has permeated across the membrane in a predetermined time Δt (h) during the tests. A_{eff} is the effective membrane surface area (m^2). C_t and V_t are the salt concentration (g/L) and the volume of the feed (L) at the end of the tests, respectively. Conductivity of the feed was measured by a ProfiLine Cond 3310 conductivity (WTW, Germany).

Determination of the Membrane Structural Parameter (*S*). The membrane structural parameter (S) is an intrinsic membrane property used to indicate the extent of internal concentration polarization (ICP) which influences the FO performance of the membranes. In the FO mode, the structural parameter is determined using

$$S = \frac{D_s}{J_v} \ln \frac{A\pi_{D,b} + B}{A\pi_{F,m} + J_v + B} \quad (9)$$

where $\mathbf{D}_s$ is the diffusivity of the draw solute, $\pi_{D,b}$ is the bulk osmotic pressure of the draw solution, and $\pi_{F,m}$ is the osmotic pressure at the membrane surface on the feed side.

Organic Fouling Tests. Bovine serum albumin (BSA) was used as a model organic foulant in this study. The adsorption propensities between the foulant and 40 mol % PTA/PSU supports were characterized by measuring the fluorescence intensity of the support surfaces after exposing to the BSA-FITC solution (0.5 mg/mL) for 1 h. The BSA-FITC adsorbed supports were captured using an epifluorescence optical microscope (Olympus BX61) with a filter at 495/520 nm. The surface density of the adsorbed BSA-FITC was further quantified using ImageJ software.

Evaluation of the Antibacterial Property. The antibacterial and biofouling resistance properties of 40 mol % PTA and PSU supports were conducted using *Pseudomonas aeruginosa* PAO1. Cultures of *Pseudomonas aeruginosa* PAO1 were grown in Luria Broth (Sigma) for 16 h, and then diluted with 0.85% w/v NaCl to an $OD600_{nm}$ of 0.06. This corresponds to a cell concentration of approximately 1×10^8 cell/mL. The membranes to be tested were cut into dimensions of 1 cm × 1.5 cm with sterilized scissors, and individually immersed into 10 mL of diluted *Pseudomonas aeruginosa* PAO1 cell suspension. The cell suspensions were incubated at 37 °C in an orbital incubator shaker for 24 h. After 24 h incubation, the cell suspensions were diluted by 2000-fold with 0.85% w/v NaCl and stained with an equal volume of 2X LIVE/DEAD BacLight bacterial viability stains for 10 min at 35 °C prior to flow cytometry on Accuri C6 (BD Biosciences). The supports were removed from the cell suspensions with sterilized forceps, placed into individual tubes of 2 mL of 0.85% w/v NaCl, and ultrasonicated for 3 min by a Q500 sonicator (Qsonica) at 25% amplitude to dislodge the attached bacteria into the suspension. After ultrasonication, the contents in the tubes were allowed to settle down for approximately 5 min. A 300 μL portion of supernatant was pipetted from each tube and individually stained with 300 μL of 2X LIVE/DEAD BacLight bacterial viability stains prior to flow cytometry. The adhered bacterial cells on the support surfaces were observed under a FESEM after the cells were fixed with a paraformaldehyde solution.

RESULTS AND DISCUSSION

Characterizations of the Porous Supports. The morphology, pore sizes, and permeation characteristics of asymmetric porous membranes are governed by the phase diagram of the polymer−solvent−nonsolvent system chosen for membrane manufacture and the path leading to phase separation. When hydrophilic polymeric units are introduced into a plain hydrophobic polyoxadiazole backbone, the phase diagram is altered. As a result, the final membrane properties such as morphology, topology, pore size, and hydrophilicity are also changed. In this paper, the effect of hydroxyl-functionalized PTA content on morphology and transport properties of the resultant PTA−POD membrane supports were investigated using four copolymers with various hydroxyl-functionalized PTA content from 0 to 50 mol % and fabricated from a similar casting solution condition containing a polymer (18 wt %) and NMP (82 wt %). In principle, the four PTA−POD derivatives have a similar number of monomers and only differ in their hydroxyl-functionalized PTA content. The 0 mol % hydroxyl-functionalized PTA based membrane support is presented as

DOI: 10.1021/am508387d
ACS Appl. Mater. Interfaces 2015, 7, 3960−3973

the POD membrane. The X mol % PTA membranes shown in this paper represent the membrane supports fabricated from PTA–POD copolymers containing X mol % of hydroxyl functionalized PTA.

Figure 2 shows the surface and cross-section morphologies of all investigated POD and PTA–POD membrane substrates with a thickness range 40–50 μm. All membranes are fully porous and asymmetric, consisting of finger-like macrovoids with interconnecting pores. The membrane thickness varies with the content of hydroxyl-functional PTA despite using the same height during the casting. The membrane as a whole tends to be thinner when the copolymer has a higher content of hydroxyl-functionalized PTA. This is due to the fact that the POD polymer is much more hydrophobic than the PTA-modified copolymers. Therefore, solutions made from the former tend to phase separate faster than the latter and result in a thicker membrane. In contrast, solutions of hydrophilic copolymers are expected to tolerate higher water content before they start to phase separate. Phase separation will only start after large part of the solvent diffuses into the water bath, leaving a denser and thinner porous membrane.

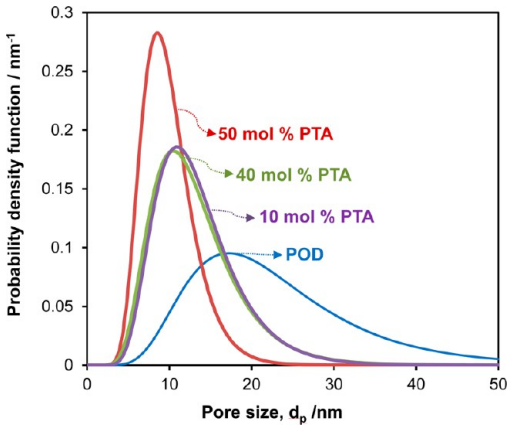

Figure 3. Pore size distribution of POD, 10 mol % PTA, 40 mol % PTA, and 50 mol % PTA porous supports.

Figure 3 and Table 1 show the pore size characteristics of these POD and PTA–POD substrates. The pore sizes and MWCO of pure POD and PTA–POD membrane substrates follow this order: POD > 10 mol % PTA > 40 mol % PTA > 50% PTA. Also, the pure water permeance values follow the same trend (Figure 4). Since systems with more hydrophilic copolymers are expected to tolerate higher water content before starting phase separation, they have different phase inversion paths and result in different pore sizes and permeance values. An additional factor leading to different pore size distributions as depicted in Figure 3 might be due to different degrees of water-induced swelling because of different PTA–OH content in these membranes. Hydrophilic copolymers might suffer some extent of swelling in water and reduce their effective pore sizes. The hydrophilicity of supports prepared from different copolymers is compared in Figure 4. Increasing the content of hydroxyl-functionalized PTA in the copolymer leads to a decrease in water contact angle. The higher hydrophilicity of the hydroxyl-functionalized triazole molecules facilitates the stronger affinity between the membranes and water. By adding 50 mol % PTA to the original POD polymer, the contact angle of the resultant porous membrane decreases from 110.3° to 83.7°.

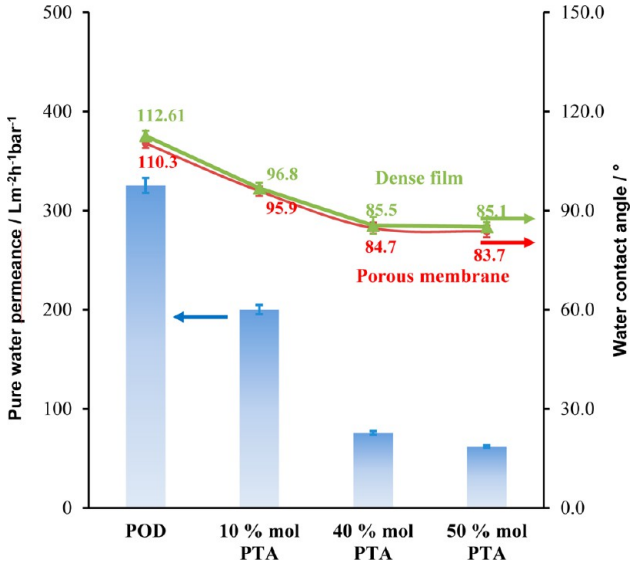

Figure 4. Comparison between pure water permeance (PWP) and contact angle as a function of substrate materials.

The final aim of this study is to use the PTA–POD membranes as substrates for TFC FO membranes. The PTA–POD porous supports manufactured here have the following characteristics, which have been considered as essential requirements for successful forward osmosis membrane supports:[45,46,48,49] (1) high water permeance, (2) low water contact angle, (3) relatively narrow pore size distributions, (4) mean pore diameters (μ_p) in the range 9.4–20.9 nm, (5) geometric standard deviations (σ_p) of approximately 1.5, and (6) high porosity (66.8–74.4%).

Effect of the Hydroxyl-Functionalized PTA Content on the Formation of the TFC Layers. Figure 5 shows the polyamide morphology formed on the POD and PTA–POD supports. Compared to the top surfaces of porous supports, the top surfaces of TFC membranes are fully covered by a layer of ridge-valley or globular structures, which indicate the successful formation of polyamide layers via interfacial polymerization.

Figure 5 also shows that these TFC layers have different roughnesses and thicknesses. The POD–TFC membrane has the roughest surface with a larger globular structure, while the 50 mol % PTA–TFC one has the smoothest TFC layer. In other words, an increase in hydroxyl-functionalized PTA

Table 1. Summary of Mean Effective Pore Diameter, Geometric Standard Deviation, MWCO, and Porosity of Substrates

POD–PTA substrate composition	mean pore diameter μ_p (nm)	geometric standard deviation σ_p	MWCO (10^3 g/mol)	porosity (%)
100% POD	20.9	1.56	257	66.8
10 mol % PTA	12.5	1.44	97	73.8
40 mol % PTA	12.2	1.47	97	76.5
50 mol % PTA	9.4	1.37	52	74.4

DOI: 10.1021/am508387d
ACS Appl. Mater. Interfaces 2015, 7, 3960–3973

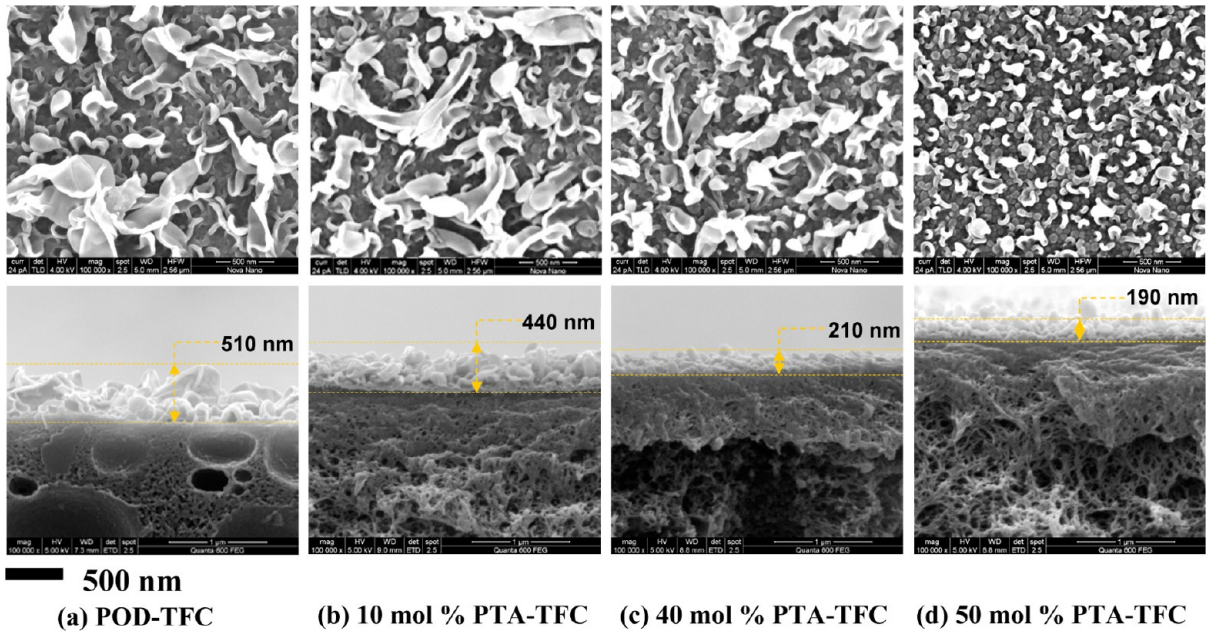

Figure 5. Morphology of FO membranes prepared with different supports: (a) POD-TFC, (b) 10 mol % PTA-TFC, (c) 40 mol % PTA-TFC, and (d) 50 mol % PTA-TFC.

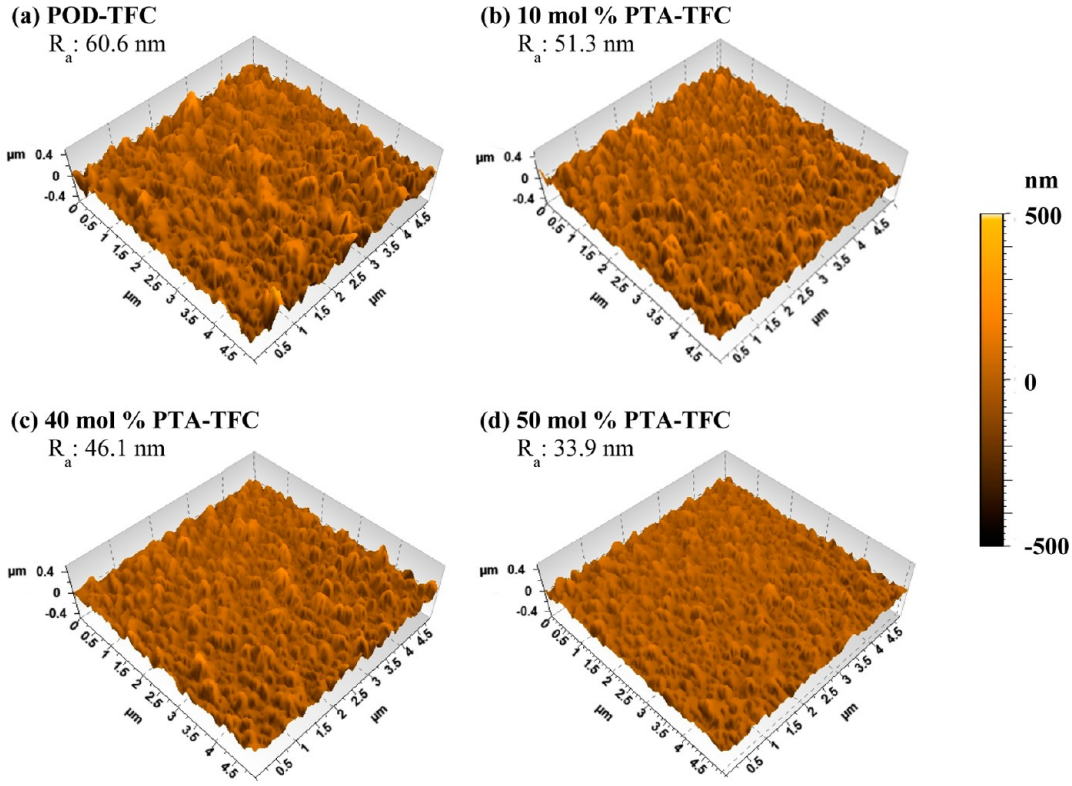

Figure 6. AFM images of FO membranes: (a) POD-TFC, (b) 10 mol % PTA-TFC, (c) 40 mol % PTA-TFC, and (d) 50 mol % PTA-TFC.

content in the substrates results in TFC membranes with a smoother polyamide surface. The thickness of the TFC layer also decreases with an increase in hydroxyl-functionalized PTA content in the support. These phenomena result from combinative effects of substrate's pore size, hydrophilicity, and hydrophobicity on the formation of TFC layers.[50,51]

Since the TFC layer was formed by interfacial polymerization when introducing the organic TMC solution onto the top surface of a porous support filled with aqueous MPD monomer, a thin polyamide skin is immediately formed as TMC and MPD monomers meet and react. Once the skin is formed, the polymerization is stopped. As a result, the morphology of the polyamide layer reflects the interface between the organic and liquid phases at the moment when these two monomers react. Because MPD must diffuse out from the substrate into the oil phase and react with TMC, the substrate's pore size and hydrophilicity (or hydrophobicity) affect its diffusion path, reaction rate, and the characteristics of the TFC layer. In

DOI: 10.1021/am508387d
ACS Appl. Mater. Interfaces 2015, 7, 3960−3973

Table 2. Transport Properties, Structural Parameters, and Surface Roughness of FO Membranes

membrane composition	water permeance[a] A (L m^{-2} h^{-1} bar^{-1})	salt rejection[b] R_s (%)	salt flux[b] B (L m^{-2} h^{-1})	S[c] (μm)	surface roughness (nm)	
					R_q	R_a
POD−TFC	1.983 ± 0.018	87.9 ± 0.7	0.792 ± 0.052	797	75.9	60.6
10 mol % PTA−TFC	1.837 ± 0.083	89.5 ± 0.2	0.757 ± 0.024	336	63.6	51.3
40 mol % PTA−TFC	1.355 ± 0.017	93.5 ± 0.4	0.308 ± 0.053	236	57.3	46.1
50 mol % PTA−TFC	1.308 ± 0.036	94.0 ± 0.2	0.285 ± 0.015	630	42.3	33.9

[a]Tested using DI water as feed. [b]Tested using 2000 ppm of NaCl as feed; nanofiltration mode operation at 5 bar. [c]Structural parameters were calculated on the basis of experiments under FO mode using 2 M NaCl as draw solution and DI water as feed.

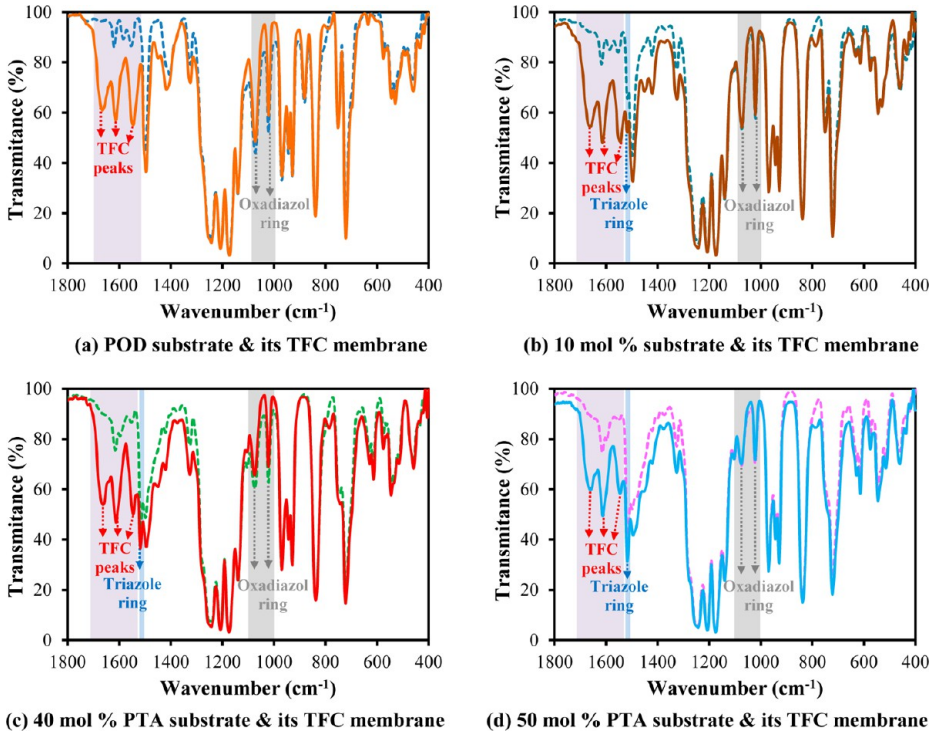

Figure 7. FTIR spectra of different substrates and corresponding TFC-FO membranes: (a) POD substrate and its TFC membrane, (b) 10 mol % PTA substrate and its TFC membrane, (c) 40 mol % PTA substrate and its TFC membrane, and (d) 50 mol % PTA substrate and its TFC membrane.

general, a substrate with a small pore and pore size distribution tends to form a flat interface and bring about a smooth TFC skin, while a substrate with a large pore and pore size distribution favors rapid mass transfer (i.e., both diffusion and convection flows) and produces a rough polyamide layer.[50] In addition, hydrophobic substrates may induce the intrusion of the organic phase into substrate pores;[51] this is especially true for the substrate made of the POD homopolymer. As a consequence, the diffusion and convective paths of MPD and TMC become complicated and result in a rough reactive interface.

Figure 6 illustrates the AFM images of the membrane surfaces, while Table 2 presents their mean roughness and root-mean-squared roughness. The roughness of polyamide layers decreases in the order POD−TFC > 10 mol % PTA−TFC > 40 mol % PTA−TFC > 50 mol % PTA−TFC. This decreasing order is consistent with the observation in FESEM analyses.

Characterizations of the TFC FO Membranes. Figure 7 shows the ATR-FTIR spectra of the supports and the active layers for all PTA−POD-based TFC membranes. The POD support spectrum in Figure 7a displays the characteristics of POD with the peaks at 1026 and 1074 cm^{-1}.[39,52] Besides the presence of peaks corresponding to the POD, the spectra of PTA−POD supports in Figure 7(b−d) exhibit an additional triazole ring peak at 1518 cm^{-1}.[53] This triazole ring peak confirms the presence of PTA in the supports. Among the investigated supports, the one with the highest PTA content also has the triazole peak with the highest intensity, while exhibiting oxadiazole peaks with the lowest intensity in the ATR-FTIR spectrum.

When the active TFC layer was added, new characteristic peaks of polyamide appear such as 1548 cm^{-1} (—N—H bending vibration of amide), 1660 cm^{-1} (—C═O stretching vibration of amide), and 1608 cm^{-1} (aromatic ring breathing of amide).[54] The results strongly indicate the successful formations of TFC layers on top of the POD and PTA−POD substrates.

Separation Properties. The separation properties of POD−PTA-based TFC membranes, including water permeance (A), salt rejection (R_s), and salt permeance (B), are summarized in Table 2. Among the TFC membranes, the POD−TFC has the largest water permeance of 1.983 L m^{-2} h^{-1} bar^{-1}, which may be due to the larger surface area associated with the rough TFC layer. Because of the smoother

DOI: 10.1021/am508387d
ACS Appl. Mater. Interfaces 2015, 7, 3960−3973

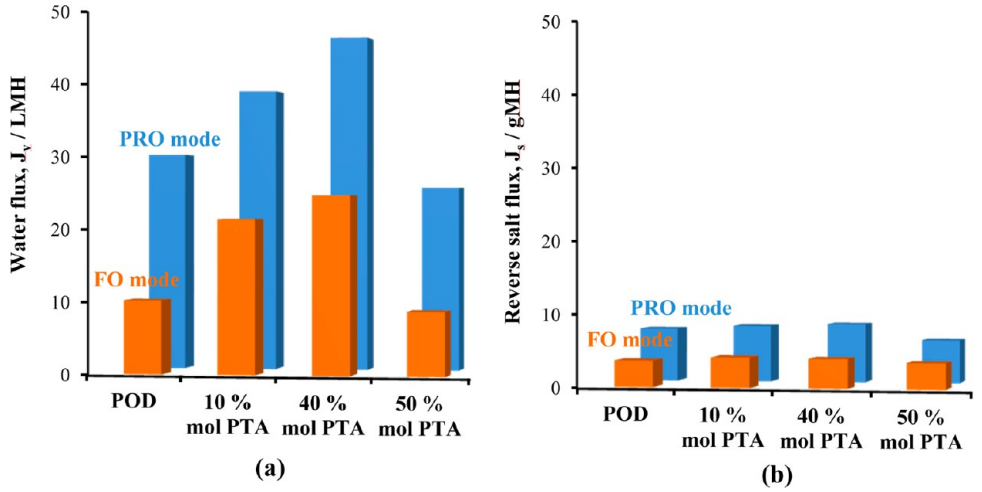

Figure 8. Comparison between (a) water fluxes and (b) reverse salt fluxes of membranes using supports with different PTA contents. DI water was used as feed; 1.0 M NaCl was used as draw solution.

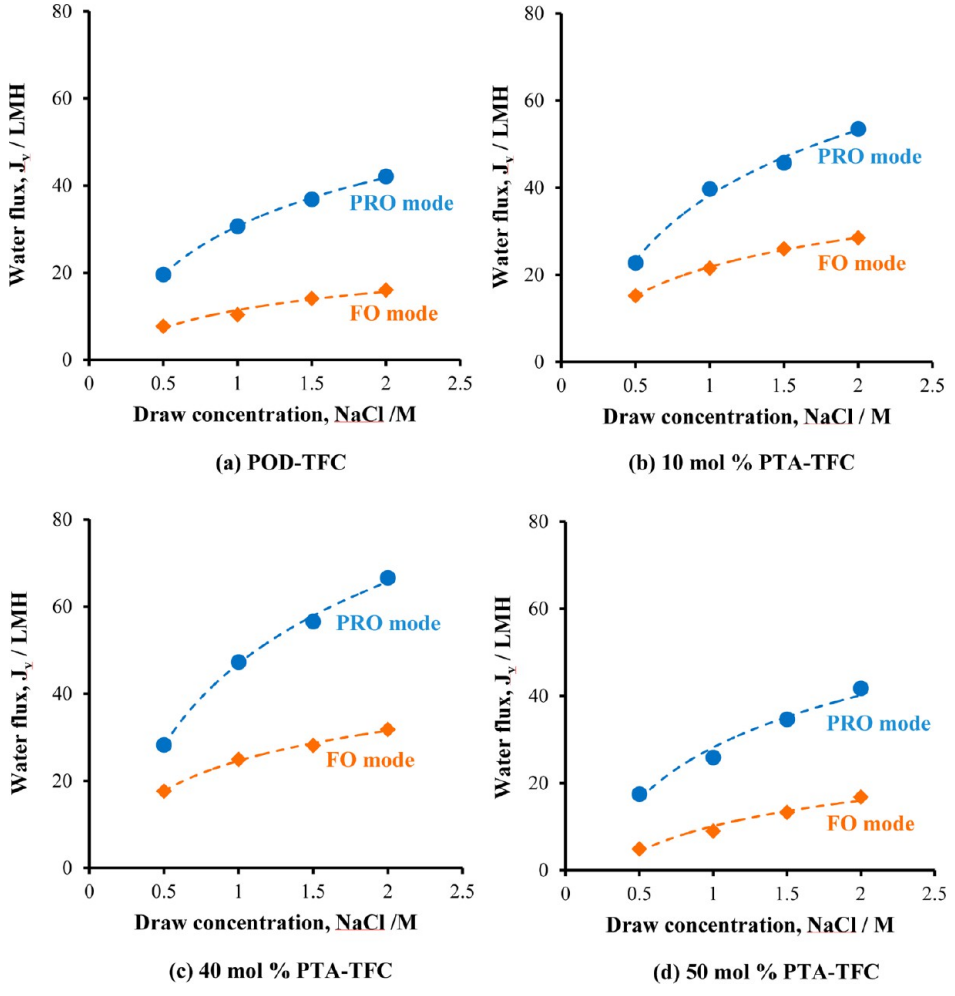

Figure 9. Water fluxes of TFC-FO membranes: (a) POD-TFC, (b) 10 mol % PTA-TFC, (c) 40 mol % PTA-TFC, and (d) 50 mol % PTA-TFC under FO and PRO testing modes using different draw solution concentrations and DI water as feed.

surfaces of TFC membranes with higher PTA content, the water permeance values become lower with the lowest value of 1.308 L m^{-2} h^{-1} bar^{-1} corresponding to the 50 mol % PTA–TFC membrane. On the contrary, the rejection toward NaCl increases from 87.9% in the POD–TFC membrane to 94% in the 50 mol % PTA–TFC membrane. The lower salt rejection in the membranes with less content of hydroxyl-functionalized PTA may be caused by (i) a less uniform dispersion of the MPD solution on the hydrophobic POD substrate and (ii) higher defect density of the TFC layer formed on the substrate with large pore sizes and wider pore size distribution.

DOI: 10.1021/am508387d
ACS Appl. Mater. Interfaces 2015, 7, 3960–3973

Evaluation of the FO Performance and Structural Parameters of POD−PTA-Based TFC Membranes. The fabricated TFC membranes with different supports were characterized in a FO cross-flow setup, using DI water as feed and various concentrations of NaCl solutions as draw solutions.

Figure 8 compares their FO performance using 1 M NaCl as the draw solution. The water fluxes in both PRO and FO modes increase with an increase in hydroxyl-functionalized PTA content in the supports from 0 to 40 mol %. Similar to the decrease of water permeance with an increase in PTA content from 40% to 50% under the pressurized filtration tests, the water fluxes of the 50 mol % PTA−TFC membrane are lower than those of the 40 mol % PTA−TFC membrane under both FO and PRO modes. The increase of water flux with increasing hydroxyl-functionalized PTA content from 0 to 40 mol % PTA agrees with results published by Widjojo et al.,[48] confirming the enhancement of FO performance by using hydrophilic polymers as supports for FO TFC membranes. Due to the high hydrophilicity and the open cell finger-like porous structure of the 40 mol % PTA substrate, its TFC membrane possesses a good water permeance (1.355 L m^{-2} h^{-1}/bar) and salt rejection (93.5%) as well as high water fluxes of 24.9 and 47.2 LMH under FO and PRO modes, respectively, while its reverse salt fluxes are of reasonable values (4.1 gMH and 8.2 gMH in FO and PRO modes, respectively).

Figure 9 displays the performance of TFC membranes as a function of draw solute concentration under both PRO and FO modes. Water fluxes increase with increasing draw solute concentration for both testing modes. The fluxes level off at higher NaCl concentrations because of more severe ICP effect at higher draw solution concentrations.

Results from FO performance (i.e., water flux and salt flux) and water permeance from NF experiments were used in eq 9 to calculate the structural parameter (S) of the porous support. As illustrated in Table 2, the calculated S value decreases as the content of hydroxyl-functionalized PTA in the substrates increases from 0 to 40 mol %. This indicates a lower ICP effect in FO experiments when the supports of the TFC membranes are more hydrophilic (Figure 4) and have larger porosity (Table 1). As the hydroxyl-functionalized PTA content increases from 40 to 50 mol %, the S value increases from 236 to 630 μm. This increase in S value reflects a combination of effects due to the decrease of porosity and formation of a thicker sponge-like top layer as part of the support. Considering the A, B, and S values of these TFC membranes, the membrane made from the support consisting of 40 mol % hydroxyl-functionalized PTA seems to be the most suitable for FO applications.

Comparison between PSU-TFC and 40 mol % PTA-TFC Membranes. Performance and fouling propensity of a TFC-FO membrane are two pervasive factors that have been focused during membrane designing for water treatment. Due to the asymmetric structure of a TFC-FO membrane, the membrane can be operated in two modes: (i) the FO mode when the TFC selective layer faces the feed solution and (ii) the PRO mode when the TFC selective layer faces the draw solution. Despite the better membrane performance under the PRO mode, the FO mode has been used in water treatment due to the less fouling propensity and the easy cleaning process of the fouled layer on the TFC layer surface caused by foulants in the feed solution. As seawater and seawater RO brine containing numerous organic compounds and microorganisms have commonly been used as draw solutions, the fouling potential of draw solutions on the support of TFC-FO membranes is also a factor to be considered during material designing of the membrane supports. In previous FO membranes, PSU has frequently been used as the TFC-FO membrane support. Hence, the newly synthesized polymer (40 mol % PTA) was cast as a support and compared to the PSU support under similar fabrication conditions for TFC FO membranes and then examined in terms of FO performance and their organic/biofouling propensity.

Table 3 compares the FO performance of TFC-FO membranes using PSU and 40 mol % PTA supports cast from polymer/NMP (18/82, w/w) solutions with the same initial casting knife height and then the same IP protocol. The FO/PRO water fluxes of the 40 mol % PTA-TFC membrane outperform the PSU-TFC membrane. It is caused by the higher permeance of the TFC layer (Table 3) formed on the 40 mol % PTA-TFC support surface which is more porous and has larger surface pores (Figure 10) than those of the PSU support surface. Compared to the 40 mol % PTA support, the PSU support has narrower macrovoid sizes and shorter lengths. As a result, the PSU support has a larger structure parameter (Table 3), which results in the more severe ICP effect and further substantiates the lower performance of the PSU-TFC membrane. This observation demonstrates that more efforts in research may possibly produce a PTA-supported FO membrane with better performance than the current developed PSU-supported membranes in the literature.[55]

Table 3. Comparison of FO/PRO Water Fluxes, Transport Properties, and Structural Parameters between PSU-TFC and 40 mol % PTA-TFC Membranes

membrane subtract	PSU-TFC	40 mol % PTA-TFC
FO water flux, J_v (L m^{-2} h^{-1})	3.2 ± 0.5	24.9 ± 1.3
PRO water flux, J_v (L m^{-2} h^{-1})	9.9 ± 0.6	47.2 ± 2.5
water permeance, A (L m^{-2} h^{-1} bar^{-1})	0.726 ± 0.011	1.355 ± 0.017
salt rejection, R_s (%)	95.9 ± 0.4	93.5 ± 0.4
salt flux, B (L m^{2-} h^{-1})	0.109 ± 0.021	0.308 ± 0.053
structural param, S (μm)	3438	236

Organic fouling behavior of the support membranes (PSU and 40 mol % PTA) was investigated by evaluating the protein adsorption propensity onto the membrane surfaces. A labeled protein, BSA-FITC, was used to quantitatively compare the amounts of adsorbed protein between the two membrane surfaces. Due to the fluorescence signal from the FITC dye in BSA-FITC, fluorescence microscopy images of protein adsorbed membranes could be captured and further quantitatively analyzed as shown in Figure 11. As clearly shown in Figure 11, the fluorescence intensity on the 40 mol % PTA membrane surface is much weaker (approximate 74% lower) than that on the PSU membrane surface. The enhanced antiorganic fouling effect of the 40 mol % PTA membrane is due to the strong repulsive force between hydroxyl groups of the polymer and BSA. It indicates the significance in antiorganic fouling property of the 40 mol % PTA membrane compared to the PSU membrane.

Bacterial growth in the presence of PSU and the 40 mol % PTA supports was studied using *Pseudomonas aeruginosa* PAO1 bacteria. The comparison was done by two methods: (i) observation of bacteria attachment to the membrane surfaces

DOI: 10.1021/am508387d
ACS Appl. Mater. Interfaces 2015, 7, 3960−3973

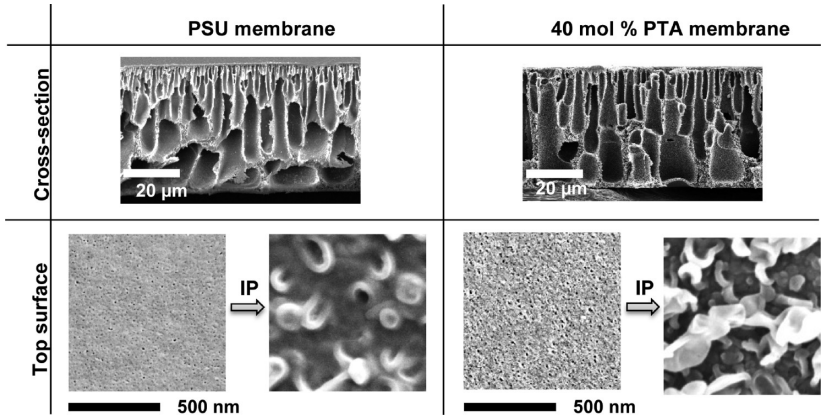

Figure 10. Comparison of morphologies between PSU and 40 mol % PTA membranes before and after the interfacial polymerization (IP).

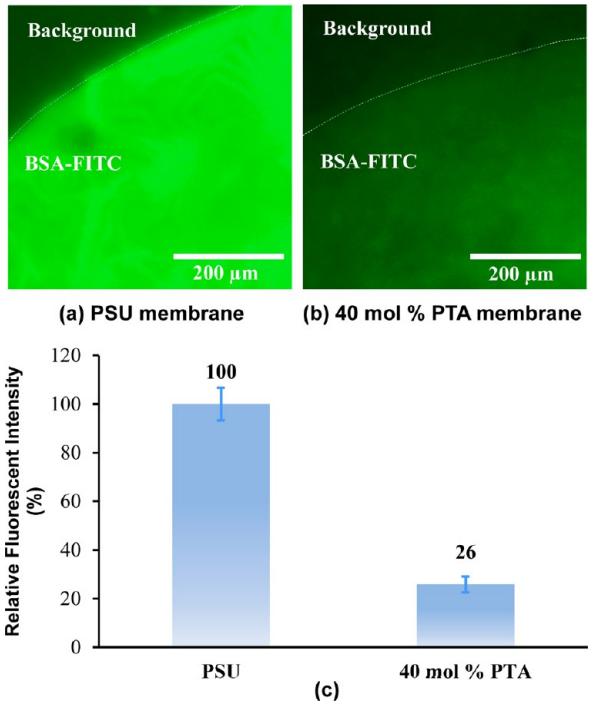

Figure 11. Fluorescence microscopy images of (a) the PSU and (b) the 40 mol % PTA supports and (c) their relative fluorescent intensity after 1 h exposure to BSA-FITC solution.

and (ii) growth inhibition of suspended + attached bacteria. The bacterial fouling propensities on membranes surfaces can be visualized from FESEM images in Figure 12. The FESEM images show that more bacterial cells are attached to the PSU support surface. However, the 40 mol % PTA support only has a low amount of bacterial attachment, suggesting a potential antibiofouling effect of the support. The low bacterial adhesion for the 40 mol % PTA support may be due to two phenomena: (i) the low bacterial adsorption caused by the hydrated ultrathin layer on the support surface, which is formed by the strong interaction between hydroxyl groups of the support and water molecules, and (ii) a potential antibacterial activity of the support that inhibits the growth of the bacteria. The result of the total bacterial growth inhibition activity is presented in Figure 12 as relative cell viability, defined as the percentage of viable suspended and attached bacterial cells with the 40 mol % PTA support sample relative to those with the PSU support sample. In comparison, the viable bacterial cells of the 40 mol % PTA support sample are only 11% of that of the PSU support sample. It indicates the antibacterial activity of the PTA support containing oxadiazole and triazole groups as expected.

Potential for Further Development of High Performance PTA-TFC FO Membranes. A polymer TFC-FO membrane is usually constituted by an asymmetric polymer support and a thin TFC selective layer. Many factors may affect the membrane performance in FO process such as the selective layer fabrication method (i.e., type of monomers, monomer concentration, preparation time, or type of organic solvents), the support material, the support fabrication method (i.e., polymer concentration, additives, type of solvents and nonsolvents and their ratios, casting thickness), and post-treatment. The effect of the support material on the TFC-FO membrane performance has been demonstrated in the previous section. Herein, a preliminary study on the effects of the support fabrication method, post-treatment, and selective layer fabrication is demonstrated specifically for the TFC-FO membranes based on 40 mol % PTA.

First, the effect of the support fabrication method was studied by a comparison taking into account the FO performance of the two 40 mol % PTA-TFC membranes fabricated from two different support structures. The pristine 40 mol % PTA-TFC membrane (referred as the nonadditive PTA-TFC membrane) contains a support fabricated from a PTA/NMP (18/82, w/w) solution while the modified ones (referred as the PEG-additive PTA-TFC membrane) consists a support cast from a PTA/PEG/NMP (18/20/62, w/w/w) solution. The differences in NaCl rejection between the nonadditive PTA–TFC membrane and the PEG-additive PTA-TFC membrane in Table 4 are attributed to the formation of the TFC selective layers on the support top layers with various surface pore sizes and porosities. The NaCl rejection increased with the addition of PEG in the support layer casting solution. This can be understood by taking into account the differences in the morphology of the two support layers shown in Figure 13. PEG as a casting solution additive for the support layer manufacture alters interfacial tension and the phase diagram promoting a more gradual, slower demixing, which favors a sponge-like structure. Smaller surface pores and a thicker sponge-like skin are seen at the top. They favor the formation of a smoother selective TFC layer with fewer defects. While the salt rejection is improved, the water permeance under the pressurized filtration test is reduced, due to the lower active surface area of the smoother selective TFC layer. Figure 3 shows that the bottom of PTA support prepared with PEG

DOI: 10.1021/am508387d
ACS Appl. Mater. Interfaces 2015, 7, 3960−3973

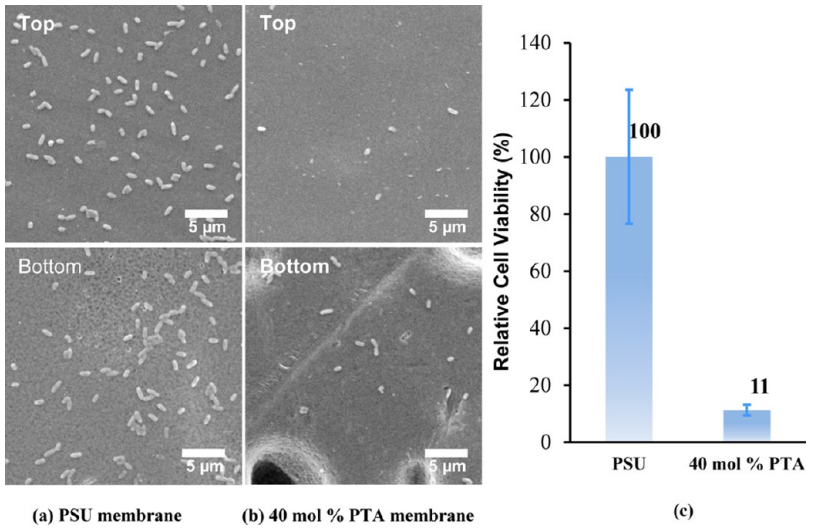

Figure 12. Bacterial adhesion on (a) the PSU and (b) the 40 mol % PTA membranes and (c) growth inhibition of suspended + attached bacteria after the membranes exposition to *Pseudomonas aeruginosa* PAO1 for 24 h.

Table 4. FO/PRO Performance and Transport Properties of 40 mol % PTA-TFC Membranes Fabricated under Different Conditions[a]

membrane subtract	post-treatment	IP method	FO water flux J_v (L m^{-2} h^{-1})	FO reverse salt flux J_s (g m^{-2} h^{-1})	PRO water flux J_v (L m^{-2} h^{-1})	PRO reverse salt flux J_s (g m^{-2} h^{-1})	water permeance A (L m^{-2} h^{-1} bar^{-1})	salt rejection R_s (%)	salt flux B (L m^{-2} h^{-1})
nonadditive	no	IP-I	24.9 ± 1.3	4.1 ± 1.5	47.2 ± 2.5	8.2 ± 2.4	1.355 ± 0.017	93.5 ± 0.4	0.308 ± 0.053
PEG-additive	no	IP-I	30.3 ± 1.2	2.9 ± 1.2	56.3 ± 1.8	5.5 ± 1.6	1.030 ± 0.083	97.3 ± 0.1	0.098 ± 0.003
PEG-additive	yes	IP-I	33.6 ± 1.8	4.4 ± 1.9	61.5 ± 1.3	8.2 ± 1.0	1.101 ± 0.017	97.0 ± 0.5	0.136 ± 0.025
PEG-additive	yes	IP-II	37.5 ± 1.3	5.5 ± 1.3	78.4 ± 2.3	12.3 ± 1.7	1.893 ± 0.029	96.8 ± 0.4	0.207 ± 0.023

[a]All FO and PRO performances were tested using DI water as feed and 1.0 M NaCl as draw.

additive has a more open structure, which may reduce the ICP effect for the membrane coated by interfacial polymerization in FO/PRO operations. As the result, enhanced FO performance with higher FO/PRO fluxes and lower reverse salt fluxes is observed in Table 4.

Second, the performance of the PEG-additive PTA-TFC membrane with and without a post-treatment process was investigated. With the post-treatment, the FO/PRO fluxes could be enhanced, while the salt rejection decreases (Table 4), but still remains acceptable for FO membrane: 97% NaCl rejection (pressurized filtration test) and <10 gMH reverse salt flux (FO/PRO tests).

Finally, two membranes with different IP methods were compared. The original IP method is referred as IP-I. The modified IP method (IP-II) corresponds to the addition of 3 wt % ethyl acetate as cosolvent for the organic phase. Compared to the IP-I method, the IP-II creates a rougher TFC layer with larger ridge-and-valley structure (Figure 13), similar to a previous study with polyamide supports.[56] The larger surface area of the TFC layer formed by the IP-II method leads to high water permeance (1.893 LMH bar^{-1}) compared to the permeance of 1.101 LMH bar^{-1} for the membrane fabricated by the IP-I method (Table 4). As a result, the membrane performance can achieve up to 37.5/78.4 LMH under FO/PRO modes, using 1 M NaCl as the draw solution.

Comparisons with Commercial and Some Reported Flat-Sheet TFC-FO Membranes. Table 5 compares the FO/PRO water flux, water permeance, and NaCl rejection of the 40 mol % PTA/PEG-additive-TFC membrane, fabricated by the IP-II method in this study and various previously reported flat-sheet TFC-FO membranes. It can be seen that the TFC-FO membrane fabricated in this study surpasses the state-of-the-art commercial membranes. Although this is the first generation of developing lab-scale PTA-TFC membranes, their performance is comparable to the best recently reported lab-scale flat-sheet TFC membranes for FO.

CONCLUSIONS

For the first time, hydroxyl-functionalized polytriazole-*co*-polyoxadiazole (PTA–POD) membranes were successfully created and subsequently used as substrates for the fabrication of FO membranes via interfacial polymerization. Four kinds of PTA–POD membranes with various hydroxyl-functionalized PTA content were demonstrated. The effects of hydroxyl-functionalized PTA content on the morphology and transport properties of the resultant substrates and the TFC membranes were investigated. Among the fabricated TFC membranes, the one prepared from 40 mol % PTA support shows the best FO performance with high water fluxes of 24.9 LMH and 47.2 LMH using 1 M NaCl as the draw solution and DI water as the feed under FO and PRO modes, respectively. Furthermore, the 40 mol % PTA support was less susceptible to fouling than the PSU support, which is the commonly used support for TFC-FO membrane. From the preliminary study on the possibilities of enhancing the FO performance of the pristine 40 mol % PTA-TFC membrane, a new 40 mol % PTA-TFC membrane with higher water fluxes of 37.5/78.4 LMH under FO/PRO modes was achieved. Further optimizations of the support fabrication, TFC layer formation, and post-treatment processes may result in 40 mol % PTA-FO membranes with even higher

DOI: 10.1021/am508387d
ACS Appl. Mater. Interfaces 2015, 7, 3960–3973

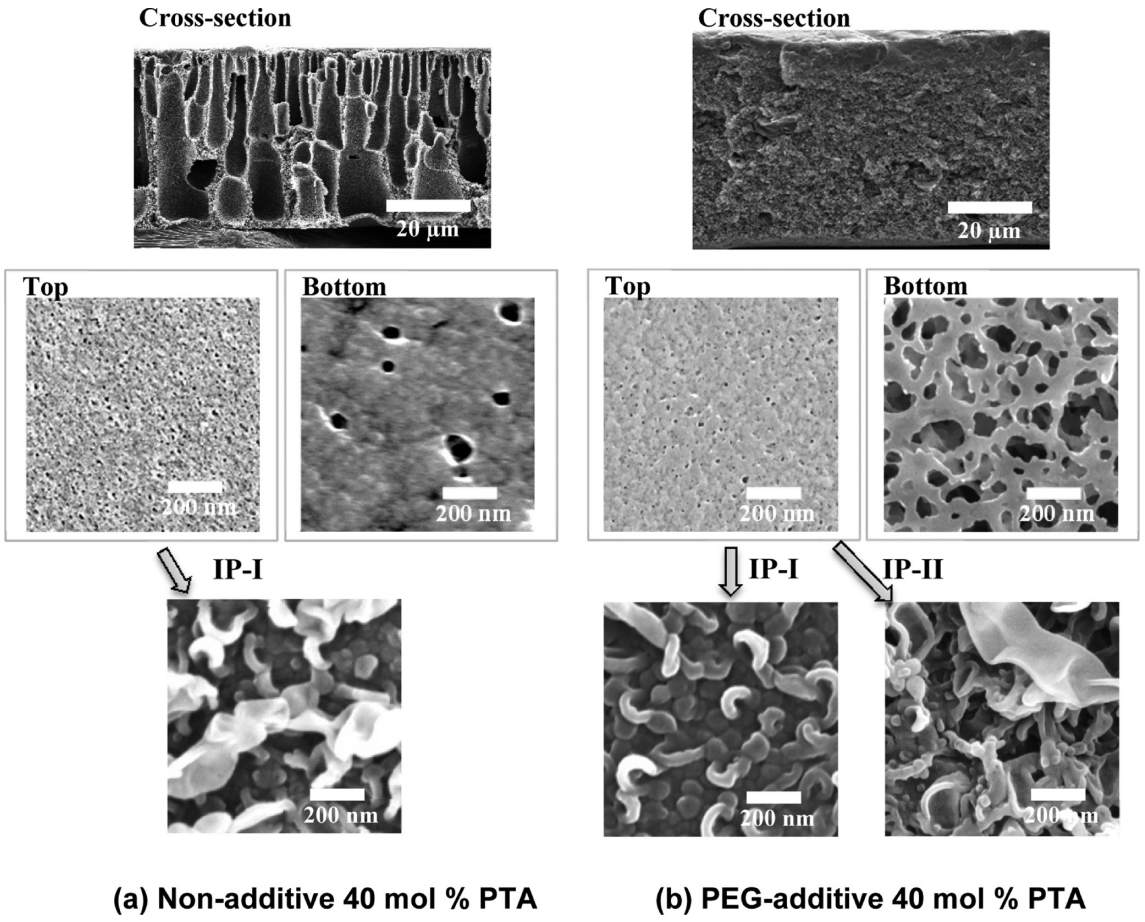

Figure 13. FESEM micrographs of 40 mol % PTA membranes at different fabrication conditions: (a, b: top and middle rows) dope compositions (nonadditive and PEG additive) and (b: last row) interfacial polymerization processes (IP-I and IP-II).

Table 5. Comparisons of FO/PRO Water Flux, Reverse Salt Flux, Water Permeance, and NaCl Rejection R_s Experimental Data of Various Flat-Sheet TFC-FO Membranes

membrane	water flux J_v FO/PRO (L m^{-2} h^{-1})	reverse salt flux J_s FO/PRO (g m^{-2} h^{-1})	feed solution	draw solution	water permeance A (L m^{-2} h^{-1} bar^{-1})	salt rejection R_s (%)	salt flux B (L m^{-2} h^{-1})	ref
40 mol % PTA/PEG additive supported TFC (IP-II)	37.5/78.4	5.5/12.3	DI water	1.0 M NaCl	1.893	96.8	0.207	this work
commercial HTI TFC, no prewetted[a]	15/30.5	4/9.5	DI water	1.0 M NaCl	1.8	91.0	1.2	57
commercial HTI TFC, prewetted[a]	15/33	7.5/17.5	DI water	1.0 M NaCl	2.45	90.5	1.65	57
Oasys TFC	23.2/–	7.8/–	0.5 mM NaCl	1.084 M NaCl	–	–	–	58
PSU supported TFC	25.0/–	–/–	DI water	1.0 M NaCl	1.90	98.6	0.33	55
PES/sulfonated PSU supported TFC	26.0/47.5	8.3/12.4	DI water	2.0 M NaCl	0.77	93.5	0.11	23
cellulose acetate propionate containing high degree of hydroxyl supported TFC	56.9/89.5	7.8/10.8	DI water	1.0 M NaCl	–	–	–	59
sulfonated polyphenylenesulfone supported TFC	48/54	7.6/8.8	DI water	2.0 M NaCl	3.23	84.1	1.05	48

[a]Data estimated from graphs.

FO performance. Clearly, POD–PTA can be used as a new class of materials for TFC membranes with demonstrated advantages of high stability, good FO performance, low organic fouling, and antibacterial activity. In addition to the performance data reported here, POD and PTA are known for their high temperature and oxidation stabilities. The newly developed TFC membranes could be potentially used for industrial applications in harsh conditions so far not addressed by the currently available supports.

AUTHOR INFORMATION

Corresponding Authors

*Phone: +966 (1) 2808 2771. E-mail: suzana.nunes@kaust.edu.sa.

DOI: 10.1021/am508387d
ACS Appl. Mater. Interfaces 2015, 7, 3960–3973

*Phone: +65 6516 6645. E-mail: chencts@nus.edu.sg.

Notes

The authors declare no competing financial interest.

■ ACKNOWLEDGMENTS

The authors would like to thank King Abdullah University of Science and Technology (KAUST) for funding this research project. Thanks are due to Dr. Russell Tayouo and Mr. Yihui Xie for their kind help.

■ REFERENCES

(1) Greenlee, L. F.; Lawler, D. F.; Freeman, B. D.; Marrot, B.; Moulin, P. Reverse Osmosis Desalination: Water Sources, Technology, and Today's Challenges. *Water Res.* **2009**, *43*, 2317−2348.

(2) Escobar, I.; Bruggen, B. V. d. *Modern Applications in Membrane Science and Technology*, 1st ed.; American Chemical Society: New York, 2011.

(3) Ben-Sasson, M.; Zodrow, K. R.; Genggeng, Q.; Kang, Y.; Giannelis, E. P.; Elimelech, M. Surface Functionalization of Thin-Film Composite Membranes with Copper Nanoparticles for Antimicrobial Surface Properties. *Environ. Sci. Technol.* **2013**, *48*, 384−393.

(4) McCloskey, B. D.; Park, H. B.; Ju, H.; Rowe, B. W.; Miller, D. J.; Chun, B. J.; Kin, K.; Freeman, B. D. Influence of Polydopamine Deposition Conditions on Pure Water Flux and Foulant Adhesion Resistance of Reverse Osmosis, Ultrafiltration, and Microfiltration Membranes. *Polymer* **2010**, *51*, 3472−3485.

(5) Lee, J.-Y.; Tang, C. Y.; Huo, F. Fabrication of Porous Matrix Membrane (PMM) Using Metal-Organic Framework as Green Template for Water Treatment. *Sci. Rep.* **2014**, *4*.

(6) Zhao, S.; Zou, L.; Tang, C. Y.; Mulcahy, D. Recent Developments in Forward Osmosis: Opportunities and Challenges. *J. Membr. Sci.* **2012**, *396*, 1−21.

(7) Alsvik, I. L.; Hägg, M. B. Pressure Retarded Osmosis and Forward Osmosis Membranes: Materials and Methods. *Polymers* **2013**, *5*, 303−327.

(8) Coday, B. D.; Yaffe, B. G. M.; Xu, P.; Cath, T. Y. Rejection of Trace Organic Compounds by Forward Osmosis Membranes: A Literature Review. *Environ. Sci. Technol.* **2014**, *48*, 3612−3624.

(9) Li, Z.; Valladares Linares, R.; Abu-Ghdaib, M.; Zhan, T.; Yangali-Quintanilla, V.; Amy, G. Osmotically Driven Membrane Process for the Management of Urban Runoff in Coastal Regions. *Water Res.* **2014**, *48*, 200−209.

(10) Lutchmiah, K.; Verliefde, A. R. D.; Roest, K.; Rietveld, L. C.; Cornelissen, E. R. Forward Osmosis for Application in Wastewater Treatment: A Review. *Water Res.* **2014**, *58*, 179−197.

(11) Qin, J. J.; Lay, W. C. L.; Kekre, K. A. Recent Developments and Future Challenges of Forward Osmosis for Desalination: A Review. *Desalin. Water Treat.* **2012**, *39*, 123−136.

(12) Chung, T. S.; Zhang, S.; Wang, K. Y.; Su, J.; Ling, M. M. Forward Osmosis Processes: Yesterday, Today and Tomorrow. *Desalination* **2012**, *287*, 78−81.

(13) Klaysom, C.; Cath, T. Y.; Depuydt, T.; Vankelecom, I. F. J. Forward and Pressure Retarded Osmosis: Potential Solutions for Global Challenges in Energy and Water Supply. *Chem. Soc. Rev.* **2013**, *42*, 6959−6989.

(14) Yangali-Quintanilla, V.; Li, Z.; Valladares, R.; Li, Q.; Amy, G. Indirect Desalination of Red Sea Water with Forward Osmosis and Low Pressure Reverse Osmosis for Water Reuse. *Desalination* **2011**, *280*, 160−166.

(15) Kim, D. Y.; Gu, B.; Kim, J. H.; Ryook Yang, D. Theoretical Analysis of a Seawater Desalination Process Integrating Forward Osmosis, Crystallization, and Reverse Osmosis. *J. Membr. Sci.* **2013**, *444*, 440−448.

(16) Coday, B. D.; Xu, P.; Beaudry, E. G.; Herron, J.; Lampi, K.; Hancock, N. T.; Cath, T. Y. The Sweet Spot of Forward Osmosis: Treatment of Produced Water, Drilling Wastewater, and other Complex and Difficult Liquid Streams. *Desalination* **2014**, *333*, 23−35.

(17) Mi, B.; Elimelech, M. Organic Fouling of Forward Osmosis Membranes: Fouling Reversibility and Cleaning without Chemical Reagents. *J. Membr. Sci.* **2010**, *348*, 337−345.

(18) Cornelissen, E. R.; Harmsen, D.; de Korte, K. F.; Ruiken, C. J.; Qin, J. J.; Oo, H.; Wessels, L. P. Membrane Fouling and Process Performance of Forward Osmosis Membranes on Activated Sludge. *J. Membr. Sci.* **2008**, *319*, 158−168.

(19) Lee, S.; Boo, C.; Elimelech, M.; Hong, S. Comparison of Fouling Behavior in Forward Osmosis (FO) and Reverse Osmosis (RO). *J. Membr. Sci.* **2010**, *365*, 34−39.

(20) Martinetti, C. R.; Childress, A. E.; Cath, T. Y. High Recovery of Concentrated RO Brines using Forward Osmosis and Membrane Distillation. *J. Membr. Sci.* **2009**, *331*, 31−39.

(21) Nguyen, A.; Azari, S.; Zou, L. Coating Zwitterionic Amino Acid L-Dopa to Increase Fouling Resistance of Forward Osmosis Membrane. *Desalination* **2013**, *312*, 82−87.

(22) Tiraferri, A.; Kang, Y.; Giannelis, E. P.; Elimelech, M. Highly Hydrophilic Thin-Film Composite Forward Osmosis Membranes Functionalized with Surface-Tailored Nanoparticles. *ACS Appl. Mater. Interfaces* **2012**, *4*, 5044−5053.

(23) Wang, K. Y.; Chung, T. S.; Amy, G. Developing Thin-Film-Composite Forward Osmosis Membranes on the PES/SPSf Substrate through Interfacial Polymerization. *AIChE J.* **2012**, *58*, 770−781.

(24) Nguyen, A.; Zou, L.; Priest, C. Evaluating the Antifouling Effects of Silver Nanoparticles Regenerated by TiO_2 on Forward Osmosis Membrane. *J. Membr. Sci.* **2014**, *454*, 264−271.

(25) Duong, P. H. H.; Zuo, J.; Chung, T. S. Highly Crosslinked Layer-by-Layer Polyelectrolyte FO Membranes: Understanding Effects of Salt Concentration and Deposition Time on FO Performance. *J. Membr. Sci.* **2013**, *427*, 411−421.

(26) Ma, N.; Wei, J.; Liao, R.; Tang, C. Y. Zeolite-Polyamide Thin Film Nanocomposite Membranes: Towards Enhanced Performance for Forward Osmosis. *J. Membr. Sci.* **2012**, *405*−*406*, 149−157.

(27) Romero-Vargas Castrillón, S.; Lu, X.; Shaffer, D. L.; Elimelech, M. Amine Enrichment and Poly(Ethylene Glycol) (PEG) Surface Modification of Thin-Film Composite Forward Osmosis Membranes for Organic Fouling Control. *J. Membr. Sci.* **2014**, *450*, 331−339.

(28) Flanagan, M. F.; Escobar, I. C. Novel Charged and Hydrophilized Polybenzimidazole (PBI) Membranes for Forward Osmosis. *J. Membr. Sci.* **2013**, *434*, 85−92.

(29) Huang, L.; McCutcheon, J. R. Hydrophilic Nylon 6,6 Nanofibers Supported Thin Film Composite Membranes for Engineered Osmosis. *J. Membr. Sci.* **2014**, *457*, 162−169.

(30) Sairam, M.; Sereewatthanawut, E.; Li, K.; Bismarck, A.; Livingston, A. G. Method for the Preparation of Cellulose Acetate Flat Sheet Composite Membranes for Forward Osmosis—Desalination using $MgSO_4$ Draw Solution. *Desalination* **2011**, *273*, 299−307.

(31) Tian, M.; Qiu, C.; Liao, Y.; Chou, S.; Wang, R. Preparation of Polyamide Thin Film Composite Forward Osmosis Membranes using Electrospun Polyvinylidene Fluoride (PVDF) Nanofibers as Substrates. *Sep. Purif. Technol.* **2013**, *118*, 727−736.

(32) Maab, H.; Nunes, S. P. Porous Polyoxadiazole Membranes for Harsh Environment. *J. Membr. Sci.* **2013**, *445*, 127−134.

(33) Maab, H.; Francis, L.; Al-saadi, A.; Aubry, C.; Ghaffour, N.; Amy, G.; Nunes, S. P. Synthesis and Fabrication of Nanostructured Hydrophobic Polyazole Membranes for Low-Energy Water Recovery. *J. Membr. Sci.* **2012**, *423*−*424*, 11−19.

(34) Gomes, D.; Nunes, S. P. Fluorinated Polyoxadiazole for High-Temperature Polymer Electrolyte Membrane Fuel Cells. *J. Membr. Sci.* **2008**, *321*, 114−122.

(35) Schulz, B.; Bruma, M.; Brehmer, L. Aromatic Poly(1,3,4-Oxadiazole)s as Advanced Materials. *Adv. Mater.* **1997**, *9*, 601−613.

(36) Gebben, B.; Mulder, M. H. V.; Smolders, C. A. Gas Separation Properties of a Thermally Stable and Chemically Resistant Polytriazole Membrane. *J. Membr. Sci.* **1989**, *46*, 29−41.

(37) Ponce, M. L.; Roeder, J.; Gomes, D.; Nunes, S. P. Stability of Sulfonated Polytriazole and Polyoxadiazole Membranes. *Asia-Pac. J. Chem. Eng.* **2010**, *5*, 235−241.

DOI: 10.1021/am508387d
ACS Appl. Mater. Interfaces 2015, 7, 3960−3973

(38) Boaventura, M.; Ponce, M. L.; Brandão, L.; Mendes, A.; Nunes, S. P. Proton Conductive Membranes Based on Doped Sulfonated Polytriazole. *Int. J. Hydrogen Energy* **2010**, *35*, 12054−12064.
(39) Singh, A. K.; Prakash, S.; Kulshrestha, V.; Shahi, V. K. Cross-Linked Hybrid Nanofiltration Membrane with Antibiofouling Properties and Self-Assembled Layered Morphology. *ACS Appl. Mater. Interfaces* **2012**, *4*, 1683−1692.
(40) Schiller, D. S.; Fung, H. B. Posaconazole: An Extended-Spectrum Triazole Antifungal Agent. *Clin. Ther.* **2007**, *29*, 1862−1886.
(41) Pearson, M. M.; Rogers, P. D.; Cleary, J. D.; Chapman, S. W.; Da Camara, C.; Perreault, M. M. Voriconazole: A New Triazole Antifungal Agent. *Ann. Pharmacother.* **2003**, *37*, 420−432.
(42) Singhal, N.; Sharma, P. K.; Dudhe, R.; Kumar, N. Recent Advancement of Triazole Derivatives and Their Biological Significance. *J. Chem. Pharm. Res.* **2011**, *3*, 126−133.
(43) Andersson Trojer, M.; Movahedi, A.; Blanck, H.; Nydén, M. Imidazole and Triazole Coordination Chemistry for Antifouling Coatings. *E-J. Chem.* **2013**, *2013*, 1−23.
(44) Chisca, S.; Duong, P. H. H.; Emwas, A. H.; Sougrat, R.; Nunes, S. P. Crosslinked Copolyazoles with a Zwitterionic Structure for Organic Solvent Resistant Membranes. *Polym. Chem.* **2015**, *6*, 543−554.
(45) Zhong, P.; Fu, X.; Chung, T. S.; Weber, M.; Maletzko, C. Development of Thin-Film Composite Forward Osmosis Hollow Fiber Membranes using Direct Sulfonated Polyphenylenesulfone (SPPSU) as Membrane Substrates. *Environ. Sci. Technol.* **2013**, *47*, 7430−7436.
(46) Widjojo, N.; Chung, T. S.; Weber, M.; Maletzko, C.; Warzelhan, V. The Role of Sulphonated Polymer and Macrovoid-Free Structure in the Support Layer for Thin-Film Composite (TFC) Forward Osmosis (FO) Membranes. *J. Membr. Sci.* **2011**, *383*, 214−223.
(47) Hatch, T.; Choate, S. P. Statistical Description of the Size Properties of Non Uniform Particulate Substances. *J. Franklin Inst.* **1929**, *207*, 369−387.
(48) Widjojo, N.; Chung, T. S.; Weber, M.; Maletzko, C.; Warzelhan, V. A Sulfonated Polyphenylenesulfone (SPPSU) as the Supporting Substrate in Thin Film Composite (TFC) Membranes with Enhanced Performance for Forward Osmosis (FO). *Chem. Eng. J.* **2013**, *220*, 15−23.
(49) Ma, N.; Liu, C.; Wang, P. J.; Tang, C. Y. Study on Nanocomposite Membranes with Enhanced Performance for Forward Osmosis. *Adv. Mater. Res.* **2014**, *900*, 191−196.
(50) Li, X.; Wang, K. Y.; Helmer, B.; Chung, T. S. Thin-Film Composite Membranes and Formation Mechanism of Thin-Film Layers on Hydrophilic Cellulose Acetate Propionate Substrates for Forward Osmosis Processes. *Ind. Eng. Chem. Res.* **2012**, *51*, 10039−10050.
(51) Ghosh, A. K.; Hoek, E. M. V. Impacts of Support Membrane Structure and Chemistry on Polyamide−Polysulfone Interfacial Composite Membranes. *J. Membr. Sci.* **2009**, *336*, 140−148.
(52) Gomes, D.; Roeder, J.; Ponce, M. L.; Nunes, S. P. Characterization of Partially Sulfonated Polyoxadiazoles and Oxadiazole-Triazole Copolymers. *J. Membr. Sci.* **2007**, *295*, 121−129.
(53) Huang, S. T.; Liaw, D. J.; Hsieh, L. G.; Chang, C. C.; Leung, M. K.; Wang, K. L.; Chen, W. T.; Lee, K. R.; Lai, J. Y.; Chan, L. H.; Chen, C. T. Synthesis and Electroluminescent Properties of Polyfluorene-Based Conjugated Polymers Containing Bipolar Groups. *J. Polym. Sci., Part A: Polym. Chem.* **2009**, *47*, 6231−6245.
(54) Duong, P. H. H.; Chung, T. S.; Wei, S.; Irish, L. Highly Permeable Double-Skinned Forward Osmosis Membranes for Anti-Fouling in the Emulsified Oil-Water Separation Process. *Environ. Sci. Technol.* **2014**, *48*, 4537−4545.
(55) Tiraferri, A.; Yip, N. Y.; Phillip, W. A.; Schiffman, J. D.; Elimelech, M. Relating Performance of Thin-Film Composite Forward Osmosis Membranes to Support Layer Formation and Structure. *J. Membr. Sci.* **2011**, *367*, 340−352.
(56) Kamada, T.; Ohara, T.; Shintani, T.; Tsuru, T. Controlled Surface Morphology of Polyamide Membranes via the Addition of Co-Solvent for Improved Permeate Flux. *J. Membr. Sci.* **2014**, *467*, 303−312.
(57) Ren, J.; McCutcheon, J. R. A New Commercial Thin Film Composite Membrane for Forward Osmosis. *Desalination* **2014**, *343*, 187−193.
(58) Tiraferri, A.; Yip, N. Y.; Straub, A. P.; Romero-Vargas Castrillon, S.; Elimelech, M. A Method for the Simultaneous Determination of Transport and Structural Parameters of Forward Osmosis Membranes. *J. Membr. Sci.* **2013**, *444*, 523−538.
(59) Ong, R. C.; Chung, T. S.; de Wit, J. S.; Helmer, B. J. Novel Cellulose Ester Substrates for High Performance Flat-Sheet Thin-Film Composite (TFC) Forward Osmosis (FO) Membranes. *J. Membr. Sci.* **2015**, *473*, 63−71.

DOI: 10.1021/am508387d
ACS Appl. Mater. Interfaces 2015, 7, 3960−3973